ACS OMEGA

Open Access

http://pubs.acs.org/journal/acsodf

Article

Computational Elucidation of Human β-Defensin-2 as a Dual Inhibitor of MMP-9 and PKC-βII for Diabetic Wound Management

Vidyasrilekha Sanapalli, Dilep Kumar Sigalapalli, Afzal B. Shaik, Richie R. Bhandare,* and Bharat Kumar Reddy Sanapalli*

Cite This: *ACS Omega* 2025, 10, 3575−3584

Read Online

ACCESS | Metrics & More | Article Recommendations | Supporting Information

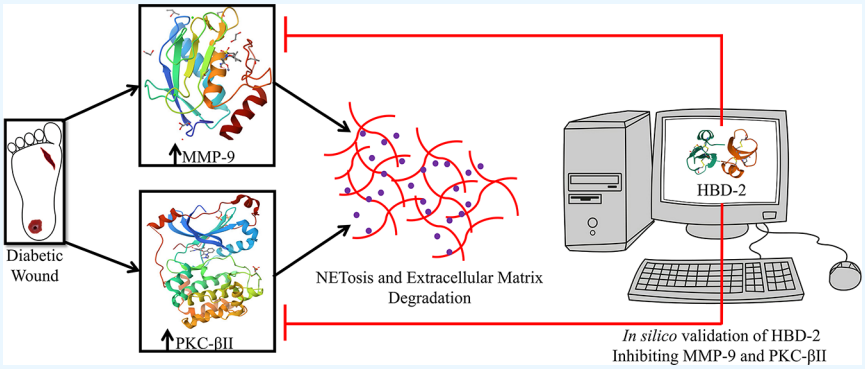

ABSTRACT: Diabetic wounds (DWs) are the most devastating complication, resulting in significant mortality and morbidity in diabetic patients. Although the pathophysiology of DWs is multifaceted, evidence has revealed that prolonged inflammation with infections, extracellular matrix (ECM) degradation, and unnecessary NETosis impair DW healing. This theoretical problem highlights the necessity of developing a novel strategy focused on targeting the "specific" molecular modalities of DWs. The primary culprits, matrix metalloproteinase (MMP)-9 and protein kinase C (PKC)-βII, are responsible for impaired angiogenesis, NETosis, and ECM degradation. Thus, interest in identifying selective inhibitors for the effective management of DW has increased. The current study exemplified human β-defensin-2 (HBD-2), a biological macromolecule that functions as a dual inhibitor of MMP-9 and PKC-βII, via protein−protein docking and molecular dynamics simulation studies. Overall, the data analysis revealed that HBD-2 possesses strong binding affinity and stability against MMP-9 and PKC-βII, suggesting that HBD-2 may be an ideal therapeutic for the accelerated healing of DW. Our findings suggest HBD-2's potential as an innovative therapeutic for accelerated DW healing, offering valuable insights into its molecular mechanisms. However, in vitro and in vivo studies are required to bridge the gap between computational modeling and clinical application.

1. INTRODUCTION

Diabetic wounds (DWs) are late-stage complications of diabetes mellitus (DM) that emanate from the interplay among inflammation, vasculopathy, neuropathy, and impaired tissue regeneration, all against the background of insulin resistance.[1,2] These wounds are notoriously difficult to heal, often leading to chronic, nonhealing states that impose a heavy burden on healthcare systems and significantly reduce patients' quality of life. According to statistics from the International Diabetes Federation, 25% of diabetic patients tend to develop DWs in their lifetime. The treatment of DW is complex because optimization of glycemic control has little or no effect; hence, the unique etiopathogenic connotation between DM and DW becomes less relevant at later phases of disease progression.[3] This theoretical problem highlights the necessity of developing a novel strategy focused on targeting the "specific" molecular modalities of DWs.

Current treatments, such as advanced wound dressings, pressure offloading, wound debridement, and patient education, often fall short because of the multifactorial nature of DWs.[4] Recent advances have introduced new strategies to enhance DW healing by focusing on molecular pathways and regenerative medicine.[5] Advanced wound dressings—such as foams, hydrogels, and bioengineered skin substitutes—support a moist wound environment that fosters cellular activity and healing.[6] Furthermore, therapies such as oxygen therapy and negative pressure wound therapy improve circulation and

Received: September 9, 2024
Revised: December 27, 2024
Accepted: January 3, 2025
Published: January 26, 2025

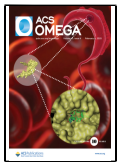

reduce the bacterial load, thus promoting wound healing.[7] In addition, regenerative therapies, including stem cell applications, growth factors (e.g., platelet-derived growth factor, epidermal growth factor, and fibroblast growth factor), and gene therapies are being applied to stimulate cellular proliferation and differentiation, addressing the core healing deficits in DWs.[8] However, recent advances are still in pipeline and are not economical while addressing aspects of the multifactorial nature of DWs. This underscores the need for a molecularly targeted approach to treatment.

The major pathogenic manifestations of impaired healing in DW are an abnormal neutrophil response to injury and insufficient vascular supply, causing prolonged inflammation and recurrent tissue damage.[9] In general, an extracellular trap (NET) is formed by active neutrophils with proteins and chromatin granules to protect the wound from infection.[10−12] However, in DW, various pathological conditions desensitize neutrophils and favor cellular death by releasing nuclear materials within NETs (NETosis).[13,14]

Gratifyingly, many studies have shown that NETosis and angiogenesis are controlled by the single enzyme protein kinase C-βII (PKC-βII).[15−18] Owing to excess glycolytic and diacylglycerol production under diabetic conditions, PKC-βII levels are increased, and its accumulation results in impaired NETosis and angiogenesis by desensitizing neutrophils and downregulating endothelial nitric oxide synthase, respectively.[15−17,19,20]

In addition, one additional cause of prolonged inflammation in DW is matrix metalloproteinase (MMP)-9, which is highly expressed in inflammatory cells and wound cells.[21] Elevated levels of this enzyme degrade the formed ECM, which delays DW healing.[22,23]

In this context, inhibiting PKC-βII and MMP-9 with a single therapeutic agent might be more effective in targeting the multifaceted DWs. Inhibiting PKC-βII and MMP-9 simultaneously could present an effective strategy by modulating inflammation, supporting angiogenesis, and stabilizing the ECM to improve healing outcomes. Such targeted approaches have the potential to address the unique etiopathogenic challenges of DWs, offering new avenues for effective management and better quality of life for diabetic patients.

Antimicrobial peptides (AMPs) are a type of innate immune system capable of fighting against infections.[24,25] AMPs have been identified as a potential new antimicrobial class, partly because of their lower susceptibility to bacterial resistance evolution. In addition, they have also been recognized for their potent wound healing activity.[26,27] Human beta defensins (HBDs) are well-categorized AMPs with broad-spectrum activity and are predominantly secreted from leukocytes and epithelial tissues. These are of six types: HBD-1, HBD-2, HBD-3, HBD-4, HBD-5, and HBD-6. Among them, HBDs (1−4) are recognized in various parts of the human body, and HBDs (5&6) have been identified recently in the human epididymis.[28] HBD-1 is constitutively expressed in various tissues and exhibits broad-spectrum antimicrobial activity, contributing to baseline immune defense. HBD-2 is inducible in the skin, epithelium, and mucous and responds to infection and inflammation, demonstrating potent activity against Gram-negative bacteria and playing a role in wound healing. HBD-3 also shows broad-spectrum activity and is effective against multidrug-resistant bacteria while also recruiting and activating immune cells.[29] HBD-4 is primarily found in the male urogenital tract and may protect against uropathogenic bacteria.[29] HBD-5 is expressed predominantly in kidney and urinary tract.[30] Finally, HBD-6, though less studied, is expressed in paneth cells and has antimicrobial activity.[29] Together, these defensins highlight the complexity and specificity of the immune response, emphasizing their potential therapeutic applications in conditions such as DWs and infections.

HBD-2 is a cationic, antimicrobial peptide discovered in 1976 that is a part of innate and adaptive immunity. It comprises 41 amino acids with a gene of 4 kb and is expressed mainly in the skin, epithelium, and mucous. In general, HBD-2 consists of six cysteine residues at positions 1−5, 2−4, and 3−6, united by three disulfide bridges.[31−33] The secondary structure of HBD-2 reveals the presence of an α-helix and three β-sheets organized in an antiparallel mode in the N-terminal region and C-terminal region (Figure 1).

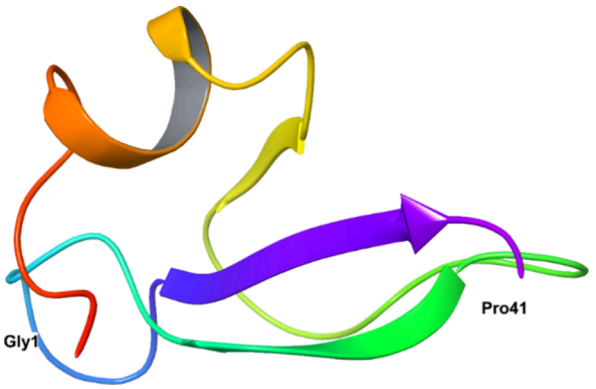

Figure 1. Crystal structure of HBD-2 with the first (Gly1) and terminal (Pro41) amino acid residues exposed.

The basic folding of the peptide is possible via disulfide bonds between the α-helix and the first β-sheet, which possess a Gly-X-CysIV domain. Although the active site is present in the N-terminal region, the antimicrobial activity of the peptide is due mainly to the presence of cationic residues present in the C-terminal region of the peptide. The remaining biological properties of the peptide are dependent on the specific conformation of the N-terminal region of HBD-2. Furthermore, its amphipathic nature and the presence of disulfide bridges are responsible for resistance to degradation by proteases.[34,35] Hence, HBD-2, a biological macromolecule, was selected as a ligand for preliminary computational studies with the goal of accelerating DW healing by inhibiting the enzymes PKC-βII and MMP-9.

2. MATERIALS AND METHODS

2.1. Protein−Protein Docking Studies. The protein 3D X-ray crystal structures of MMP-9 and PKC were retrieved from the RCSB-PDB database with PDB IDs of 4XCT and 2I0E. To confirm the reliability and quality of these structures, validation was performed via PROCHECK to evaluate stereochemical parameters and ProSA-web to analyze Z scores, ensuring the conformational stability of each structure.[36,37] For energy refinement, hydrogen atoms were added to each protein structure to eliminate potential steric hindrances, and partial atomic charges were assigned. This preparation step optimized the electrostatic properties essential for accurate molecular interactions in the docking studies. The assignment of partial

https://doi.org/10.1021/acsomega.4c08292
ACS Omega 2025, 10, 3575−3584

charges was guided by the AMBER parameters to simulate physiological conditions.

The ligand used in these studies, HBD-2, was also obtained from the RCSB PDB. Its structure was treated similarly to ensure consistency across all the prepared proteins; any missing atoms were added, and energy minimization was conducted to stabilize the ligand structure. For the protein−protein docking experiments, Discovery Studio's Z-DOCK (http://zdock.umassmed.edu/) protocol was used to explore the binding orientations between MMP-9, PKC-βII, and HBD-2. Z-DOCK's grid-based approach employs a shape-complementarity scoring algorithm, which facilitates a thorough exploration of the binding poses. For each docking run, 2000 poses were generated with an angular increment of 15° to maximize the sampling accuracy. The default parameters were maintained for reproducibility, including setting parallel processing to "False" to enable sequential execution and enabling Z-Rank to refine docking scores, which improved the selection of the most energetically favorable protein−protein complexes. The binding poses were ranked on the basis of docking scores, and the highest-scoring complexes were analyzed in detail. Visualization of interactions was performed via PDBSUM, which provided insights into the structural relationships among MMP-9, PKC-βII, and HBD-2. This comprehensive approach ensured the accuracy of the predictions regarding the structural stability and binding affinity of these complexes.

2.2. Molecular Dynamics Simulation (MDS) Studies. The complex structures of MMP-9 and PKC-βII with HBD-2 as a ligand protein identified from the Z-Dock pose were subjected to MDS studies to gain deeper insights into binding stability. Compared with docking studies, MDS studies provide a more dynamic and comprehensive view, allowing the observation of the conformational behavior of ligands over time within the catalytic pocket.[38] System preparation of both complexes was carried out via the procedure reported by Gangadharappa et al., 2020 and Prasanth et al., 2021.[39,40] The system was neutralized by adding counterions and solvated via the TIP3P water model. The simulation protocol included an initial energy minimization step to resolve any unfavorable interactions in the starting model, followed by equilibration at constant temperature and pressure to prepare the system for the production run. The GROMACS simulation package was used to analyze the simulated data of the two complexes. The production simulations were run for 1000 ns with trajectory snapshots collected at regular intervals, providing data on key stability metrics such as the root-mean-square deviation (RMSD), root-mean-square fluctuation (RMSF), and hydrogen bonding patterns. RMSD and RMSF were employed to analyze the backbone atoms and C-α fluctuations, respectively. Furthermore, the radius of gyration was computed to determine the "extendedness" of the protein residues. All these calculations were performed via various methods, such as "gmxrms", "gmxrmsf", "gmx select", and "gmx gyrate". This detailed time-resolved information offered insights into the flexibility and stability of the ligand within the binding site, often revealing binding modes and key interactions not evident in docking studies alone. By allowing the ligand and protein complex to fluctuate naturally over time, MDS provides a more nuanced understanding of binding affinity and stability, contributing valuable context to the static docking models initially produced through Z-DOCK.

2.3. Free Energy Calculation (MM-PBSA). This method is employed to obtain insights into protein−protein interactions by calculating interaction free energies. The free energy was computed via g_mmpbsa, the utility of the gromacs.[41] This approach integrates the MM-PBSA method, allowing for precise estimation of free energies by analyzing snapshots over the course of the simulation. For accurate binding energy estimations, the final 500−1000 ns of the MD trajectories were selected, representing a stabilized segment of the simulation where the complex had equilibrated. By analyzing this stabilized portion, we minimize the effects of initial structural relaxation and fluctuations, thus enhancing the reliability of the free energy calculation. This detailed evaluation of free energy provided valuable confirmation of the MD results, validating the predicted interactions and offering a quantitative basis for the protein−protein interaction strength and stability in the bound state.

2.4. Principal Component (PC) and Free Energy Landscape (FEL) Analyses. PC is usually carried out to generate a mass-weighted covariance matrix (CM) of protein atom displacement, indicating the collective and dominant modes of the receptor throughout simulation studies of the MD trajectory.[42,43] The CM is diagonalized to extract a set of eigenvalues and eigenvectors via g_covar (GROMACS utility), which indicates concerted molecular motion. In addition, eigenvectors were analyzed and plotted via the g_anaeig tool, which is available in GROMACS.[44,45] Furthermore, the results obtained from the PC analysis were subjected to FEL analysis. The g_covar and g_anaeig utilities were employed to identify the changes in the motion patterns of both complexes.[46,47]

3. RESULTS AND DISCUSSION

3.1. Protein−Protein Docking Studies. Protein−protein docking was performed for HBD-2 (PDB ID: IFD3) against two receptors, MMP-9 (PDB ID: 4XCT) and PKC-βII (PDB ID: 2I0E), to identify potential ligands for accelerated healing of DW. Although many conformations were generated (Table 1), the top-scoring conformation was given preference and was used for further analysis. PDBsum and PyMOL visualization tools were used to analyze protein−protein interactions. Depending on the binding interactions, two conformations were selected and presented significant Z scores of −118.026 kcal/mol (4XCT) and −140.319 kcal/mol (2I0E).

Table 1. Z Scores of the Top 10 Complexes for Both the Receptors 4XCT and 2I0E

		Z score (kcal/mol)	
s. no.	poses	4XCT	2I0E
1.	pose 1	−118.026	−140.319
2.	pose 2	−115.232	−132.052
3.	pose 3	−114.756	−128.945
4.	pose 4	−113.711	−128.348
5.	pose 5	−113.289	−126.638
6.	pose 6	−113.257	−126.389
7.	pose 7	−112.061	−126.261
8.	pose 8	−111.632	−124.635
9.	pose 9	−110.688	−121.732
10.	pose 10	−109.346	−120.367

3.2. Molecular Interaction Studies of the Top-Ranked Complex HBD-2/4XCT. Protein−protein interaction analysis revealed key insights into how HBD-2 may modulate the

https://doi.org/10.1021/acsomega.4c08292
ACS Omega 2025, 10, 3575−3584

Table 2. Residue−Residue Interactions (Hydrogen Bonds) and Distance between the Bonds across the Protein−Protein Interface between Chains A (4XCT) and B (HBD-2)

s. no.	chain A (4XCT)	chain B (HBD-2)	distance (Å)
1.	Tyr179	Arg291	2.82
2.	His226	Lys308	2.08
3.	His230	Lys308	3.12
4.	His236	Lys308	2.90
5.	Tyr248	Lys279	2.24
6.	Tyr248	Lys279	1.70

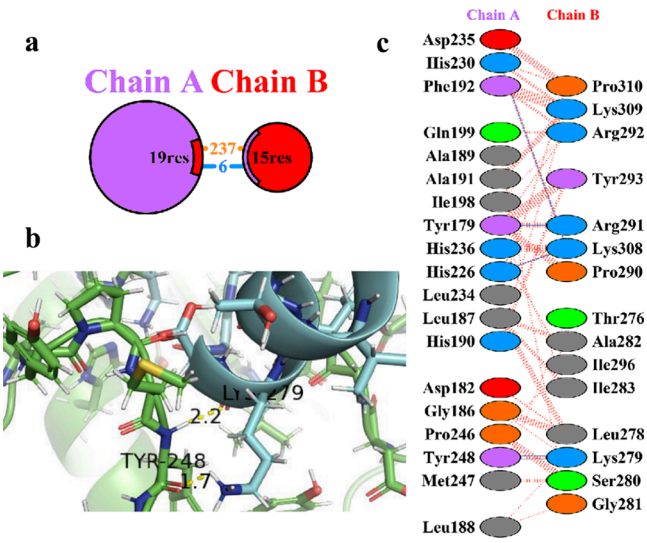

Figure 2. (a) Protein−protein interactions between chains. The area of each circle is relative to the surface area of chains A (4XCT) and B (HBD-2). (b) Residue−residue interactions across the protein−protein interface, i.e., between chains A (4XCT) and B (HBD-2). The dashed line represents nonbonded contacts, the solid blue line represents hydrogen bonds, and the solid red line represents salt bridges. (c) 3D interaction diagram depicting two hydrogen bonds across the interface of the HBD-2/4XCT complex.

Table 3. Residue−Residue Interactions (Hydrogen Bonds and Salt−Bridge Interactions) and Distances between the Bonds across the Protein−protein Interface between Chains A (2I0E) and B (HBD-2)

s. no.	chain A (4XCT)	chain B (HBD-2)	distance (Å)
Hydrogen bonding interactions			
1.	Lys468	Gln695	1.5
2.	Gly543	Lys679	2.1
Salt-bridge interactions			
1.	Asp381	Arg691	4.00
2.	Asp466	Lys694	3.92
3.	Glu542	Lys679	3.06
4.	Glu544	Lys679	3.84

activity of MMP-9 and PKC-βII, suggesting potential mechanisms underlying its effects (Table 2). The amino acid residues involved in the protein−protein interactions were obtained via the PDBsum of the 3D structure of the HBD-2/4XCT complex. From the analysis, it was clear that only 15 residues of HBD-2 (chain B) and 19 residues of 4XCT (chain A) contributed significantly to the interaction (Figure 2a). The complex exhibited a total of 6 hydrogen-bonding interactions and 237 nonbonded interactions (Figure 2b). Among the six hydrogen bonds, only two were found to be prominent, as depicted in Figure 2c. The remaining hydrogen bonds were not visible when the distance was greater than 2.5 Å. The > C═O and -NH groups of Tyr248 (4XCT) exhibited two hydrogen bonding interactions with the -NH_2 (>C = O···HN(H), 1.7 Å) and > C═O (−NH···O = C<, 2.2 Å) groups of Lys279 (HBD-2), respectively. These bonds likely contribute to stability of the complex by reinforcing the close proximity of key catalytic or regulatory regions within MMP-9. Furthermore, the presence of 237 nonbonded interactions further stabilizes this complex, potentially influencing the structural flexibility and activity of MMP-9. These findings suggest that HBD-2 may directly impact the conformation of MMP-9 and, consequently, its catalytic activity, possibly interfering with substrate accessibility or altering its binding affinity for its natural substrates.

3.3. Molecular Interaction Studies of the Top-Ranked HBD-2/2I0E Complex. The protein−protein interactions are depicted in Table 3. The protein−protein interaction residues were analyzed via PDBsum of the 3D structure of the top-ranked HBD-2/2I0E complex. During analysis, a total of 18 residues of HBD-2 (chain B) and 22 residues of 2I0E (chain A) were involved in the interactions (Figure 3a). Furthermore, the complex exhibited 2 hydrogen-bonding, 4 salt-bridge and 154 nonbonded contact interactions within the catalytic pocket of 2I0E (Figure 3b). The two hydrogen bonds were found to be prominent and are depicted in Figure 3c. The > C═O of Lys468 (chain A) formed a hydrogen bond with the side chain -NH_2 group of Gln695 (chain B) (>C = O···HN(H), 1.5 Å). Another hydrogen bond was observed between the > C═O of Gly543 (chain A) and the -NH group of Lys679 (chain B) (−NH···O = C<, 2.1 Å). The presence of nonbonded contacts and salt-bridge interactions between the residues further implies that HBD-2 could modulate the electrostatic environment of the active site of PKC-βII, potentially influencing its phosphorylation activity or altering its substrate binding affinity.

Together, these results support a model in which HBD-2 stabilizes both MMP-9 and PKC-βII through specific hydrogen bonding, nonbonding, and electrostatic interactions. By doing so, HBD-2 may exert regulatory effects on these enzymes, potentially altering their structural conformation and modulating their functional activity. These findings suggest that HBD-2 could serve as a regulatory protein that modulates the activity of MMP-9 and PKC-βII, which may be important in processes such as inflammation and the immune response, where these proteins play critical roles. Further studies are warranted to explore this regulatory mechanism and its implications in physiological and pathological contexts.

3.4. Molecular Dynamics (MD) Simulation Analysis of the HBD-2/4XCT and HBD-2/2I0E Complexes. To explore the protein−protein complex stability and dynamic properties, 1000 ns MD simulation studies were performed for each of the docked complexes. The average values of every parameter of the HBD-2/4XCT and HBD-2/2I0E complexes were calculated from their MD trajectories and are tabulated in Table 4. The analysis of simulation data utilized the GROMACS software package, with various utilities such as “gmx rms,” “gmx select,” “gmx rmsf,” and “gmx gyrate,” to compute essential stability parameters. Specifically, these tools calculate the root-mean-square deviation (RMSD) for backbone atoms, the root-mean-square fluctuation (RMSF) for Cα atoms, and

https://doi.org/10.1021/acsomega.4c08292
ACS Omega 2025, 10, 3575−3584

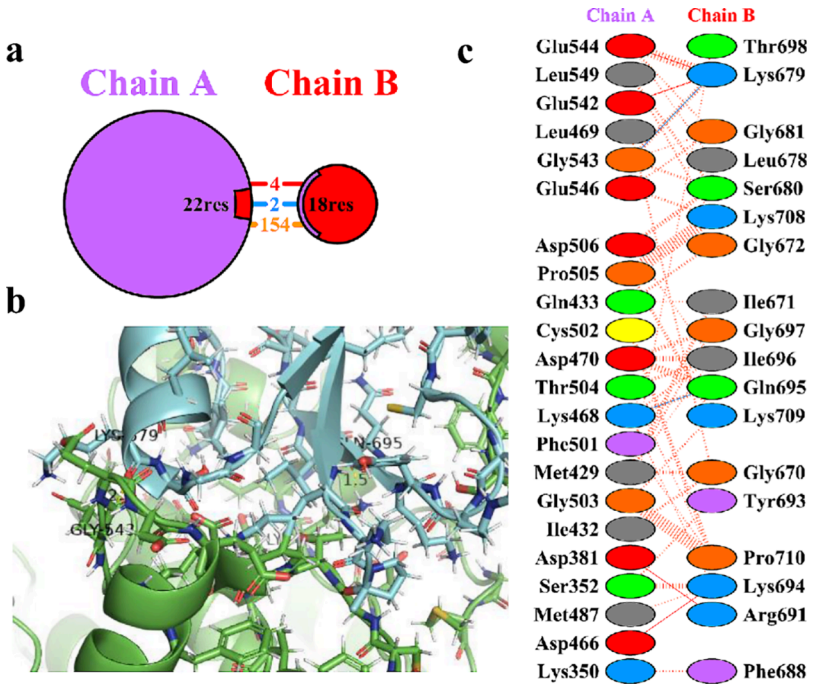

Figure 3. (a) Protein−protein interactions between chains. The area of each circle is relative to the surface area of chains A (2I0E) and B (HBD-2). (b) Residue−residue interactions across the protein−protein interface, i.e., between chains A (2I0E) and B (HBD-2). The dashed line represents nonbonded contacts, the solid blue line represents hydrogen bonds, and the solid red line represents salt bridges. (c) 3D interaction diagram depicting two hydrogen bonds across the interface of the HBD-2/2I0E complex.

Table 4. Average Values of the Root-Mean Square Deviation (RMSD), Root-Mean Square Fluctuation (RMSF), Radius of Gyration (ROG), and Solvent Accessible Surface Area (SASA) Were Calculated from 1000 ns MD Trajectories

s. no.	complex	average RMSD (nm)	average RMSF (nm)	average ROG (nm)	average SASA (nm^2)
1.	HBD-2/4XCT	0.303 ± 0.01	0.338 ± 0.098	1.633 ± 0.034	101.278 ± 0.640
2.	HBD-2/2I0E	0.399 ± 0.06	0.451 ± 0.330	2.063 ± 0.024	183.409 ± 21.349

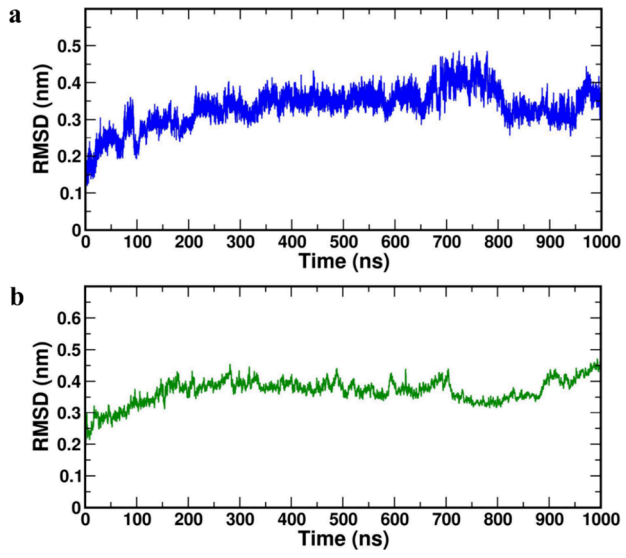

Figure 4. RMSD plot of the (a) HBD-2/4XCT (b) HBD-2/2I0E complexes during 1000 ns of MD simulation.

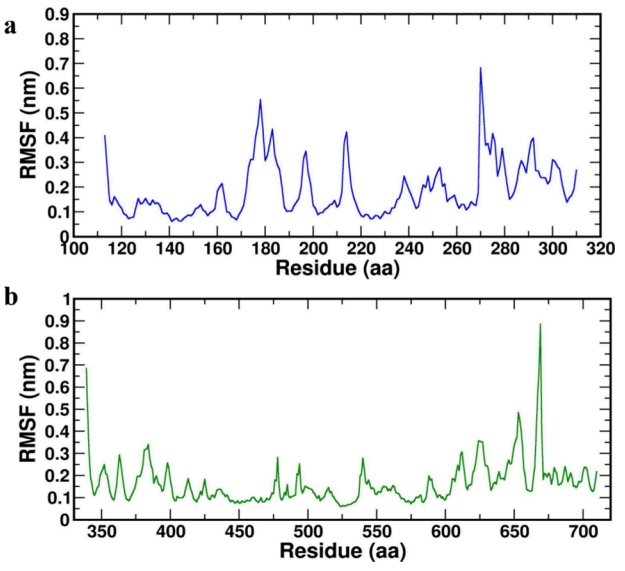

Figure 5. RMSF plot of the (a) HBD-2/4XCT (b) HBD-2/2I0E complexes during 1000 ns of MD simulation.

the radius of gyration (ROG) to evaluate each complex's stability, flexibility, and compactness, respectively.

The RMSD images depict the moving parts and spatial displacement rates of the protein model during MD simulation and serve as a measure of receptor stability.

The lower values of the RMSD correspond to protein stability during the simulation, and the acceptable average value for a protein is ≤0.4 nm. The average RMSD values for both complexes remained below 0.4 nm, confirming their stability (Table 4). RMSD diagrams were plotted over 1000 ns

https://doi.org/10.1021/acsomega.4c08292
ACS Omega 2025, 10, 3575−3584

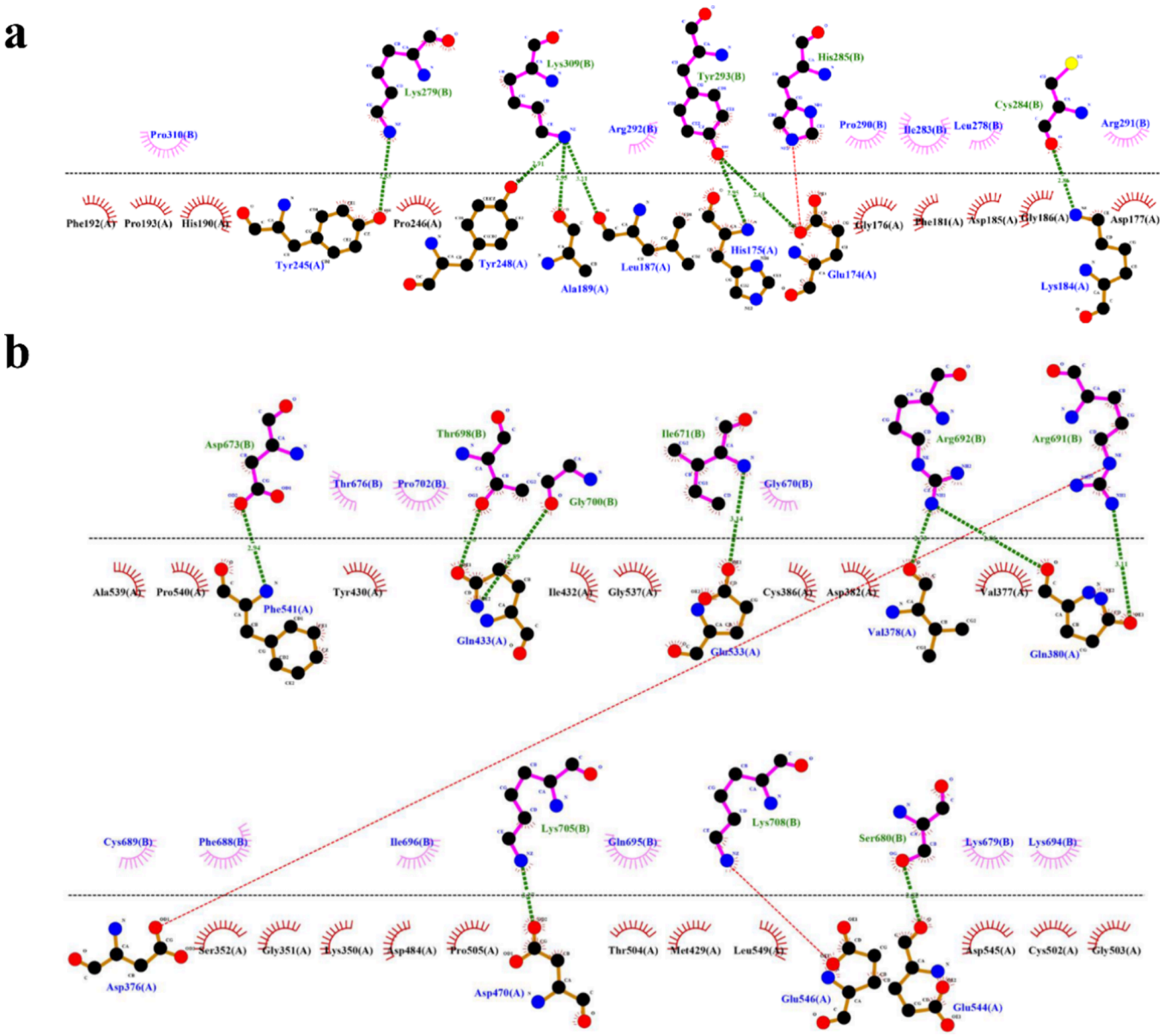

Figure 6. Protein−protein interface revealing key interactions of the complexes (a) HBD-2/4XCT; (b) HBD-2/2I0E of 1000 ns MD simulation trajectories.

of the MD study with both the HBD-2/4XCT (Figure 4a) and HBD-2/2I0E (Figure 4b) complexes. For both complexes, the systems reached equilibrium after 200 ns. The average RMSD value of the HBD-2/4XCT complex was 0.303 ± 0.01 nm, whereas for the HBD-2/2I0E complex, the value was 0.399 ± 0.06 nm.

Furthermore, the RMSF was calculated to determine the dynamic behavior of the Cα atoms and backbone flexibility of the protein, which in turn is useful for investigating each motion that corresponds to the general motion of the protein. Higher values of RMSF correspond to greater flexibility of the backbone residues during the simulation. RMSFs were plotted for both the HBD-2/4XCT (Figure 5a) and HBD-2/2I0E (Figure 5b) complexes for the 1000 ns MD study. The average RMSF values were 0.338 ± 0.098 nm and 0.451 ± 0.330 nm for HBD-2/4XCT and HBD-2/2I0E, respectively (Table 4).

In the case of HBD-2/4XCT, residues Asp185 to Pro310 lie in the catalytic pocket or protein−protein interface. A total of seven hydrogen bonding interactions were observed between the residues of HBD-2 and 4XCT (Figure 6a). In contrast, in HBD-2/2I0E, the protein−protein interface was occupied by residues Ile671 to Pro710. Approximately eight hydrogen bonding interactions were observed at the interface of the MD trajectory pose of the HBD-2/2I0E complex (Figure 6b).

The radius of gyration (ROG) parameter depicts protein structure compression or folding behavior during MD simulation. The lower ROG values of 1.633 ± 0.034 nm and 2.063 ± 0.024 nm were obtained for HBD-2/4XCT and HBD-2/2I0E, respectively (Table 4), indicating no conformation of distortion and increased compactness during the MD study (Figure 7a and 7b).

Furthermore, the protein−protein solvent-accessible surface area (SASA) was computed for both complexes and is presented in Figure 8a (HBD-2/4XCT) and 8b (HBD-2/2I0E). As SASA indicates the solvent replacement phenomenon, lower values indicate that the catalytic pocket is less

https://doi.org/10.1021/acsomega.4c08292
ACS Omega 2025, 10, 3575−3584

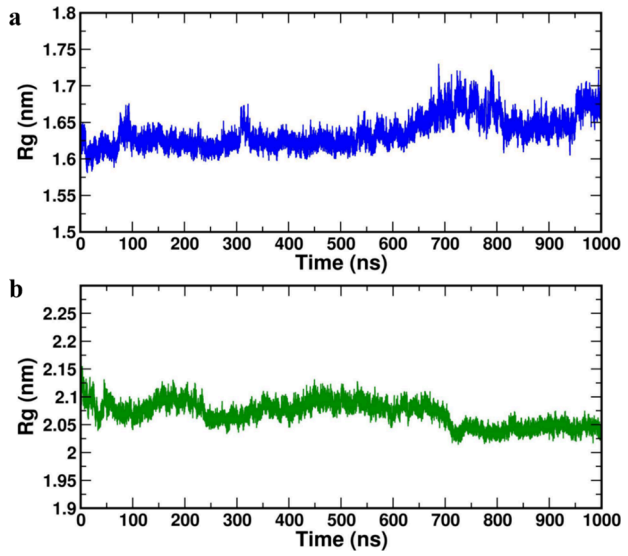

Figure 7. Radius of gyration plot of the complexes (a) HBD-2/4XCT. (b) HBD-2/2I0E during the 1000 ns MD simulation.

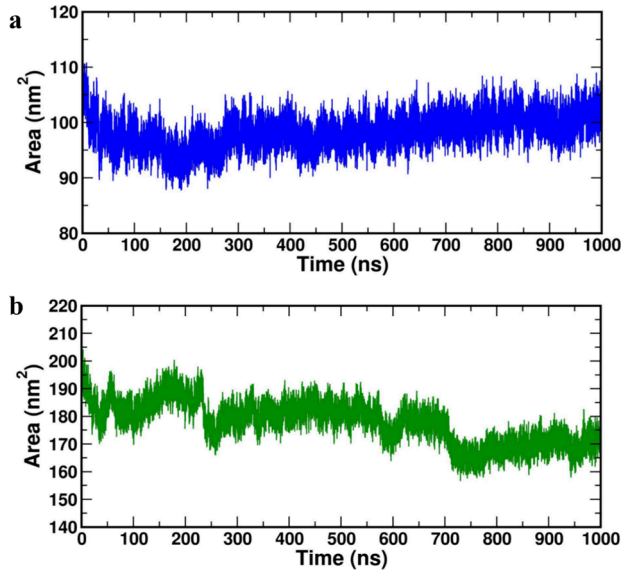

Figure 8. Solvent accessible surface area of the complexes. (a) HBD-2/4XCT. (b) HBD-2/2I0E during the 1000 ns MD simulation.

exposed to the solvent and that the ligand is retained within the catalytic site throughout the study. The average SASA values of 101.278 ± 0.640 nm^2 and 183.409 ± 21.349 nm^2 were obtained for HBD-2/4XCT and HBD-2/2I0E, respectively (Table 4), indicating that HBD-2 was deeply positioned within the binding pockets of 4XCT and 2I0E.

3.5. Binding Free Energy Calculations-MMPBSA Approach (ΔGbind). The ΔGbind was computed for both

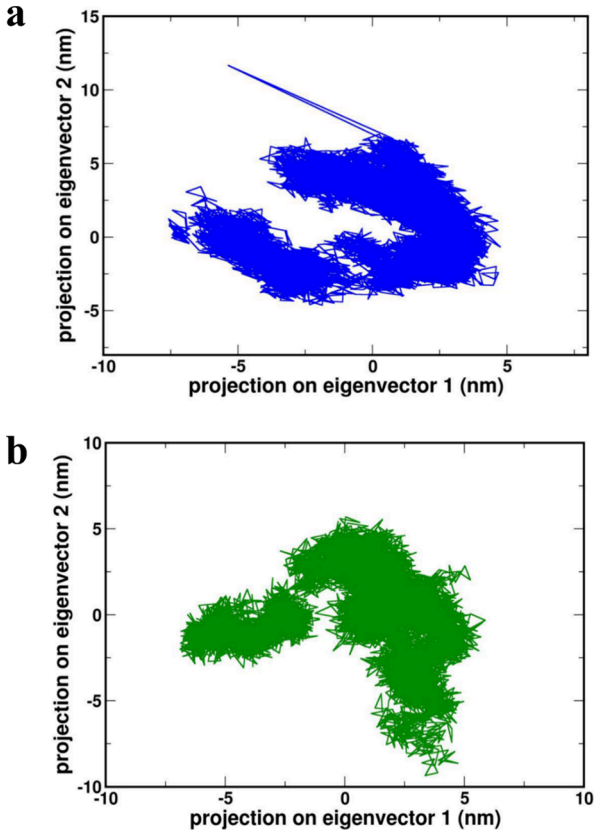

Figure 9. Projection of the motion of proteins (a) 4XCT (b) 2I0E in phase space along PC1 and PC2.

complexes for every 100 ns from the last 500 ns MD trajectories. The average values of the ΔGbind, van der Waals (Vdws), electrostatic (E), polar solvation (PS) and SASA energies were computed and are tabulated in Table 5. For the HBD-2/4XCT complex, the average ΔGbind was −2318.73 ± 35.46 kJ/mol, whereas for the HBD-2/2I0E complex, it was slightly lower at −2329.62 ± 61.24 kJ/mol, indicating the greater stability of HBD-2 within the catalytic pocket of both residues. In addition, the complexes possess significant VdWs, E, SASA and PS values, supporting the notion of effective binding affinity and substantial burial of HBD-2 within the catalytic sites. These interactions likely reflect a close fit and strong affinity of HBD-2 within the protein complexes, reinforcing the stability of HBD-2 in both binding environments.

3.6. Principal Component (PC) and Free Energy Landscape Analysis. PC analysis is a powerful approach for understanding the motion changes of complexes during MD simulation studies by analyzing concerted atomic fluctuations. The diagonalization of the covariance matrix of the Cα atom fluctuations can be analyzed through eigenvalues

Table 5. Average Values of the Molecular Mechanics Poisson−Boltzmann Surface Area-Based Energy, Van Der Waals Energy, Electrostatic Energy, Polar Solvation Energy, and SASA Energy Were Calculated for Every 100 ns of the Last 500 ns of the MD Simulation Trajectories

s. no.	complex	binding free energy (MMPBSA) (kJ/mol)	van der Waals energy (kJ/mol)	electrostatic energy (kJ/mol)	polar solvation energy (kJ/mol)	SASA energy (kJ/mol)
1.	HBD-2/4XCT	−2318.73 ± 35.46	−244.03 ± 28.47	−29.72.88 ± 35.61	929.77 ± 38.78	−31.59 ± 2.58
2.	HBD-2/2I0E	−2329.62 ± 61.24	−415.49 ± 33.27	−3448.1 ± 171.41	1588.83 ± 171.95	−54.85 ± 3.82

https://doi.org/10.1021/acsomega.4c08292
ACS Omega 2025, 10, 3575−3584

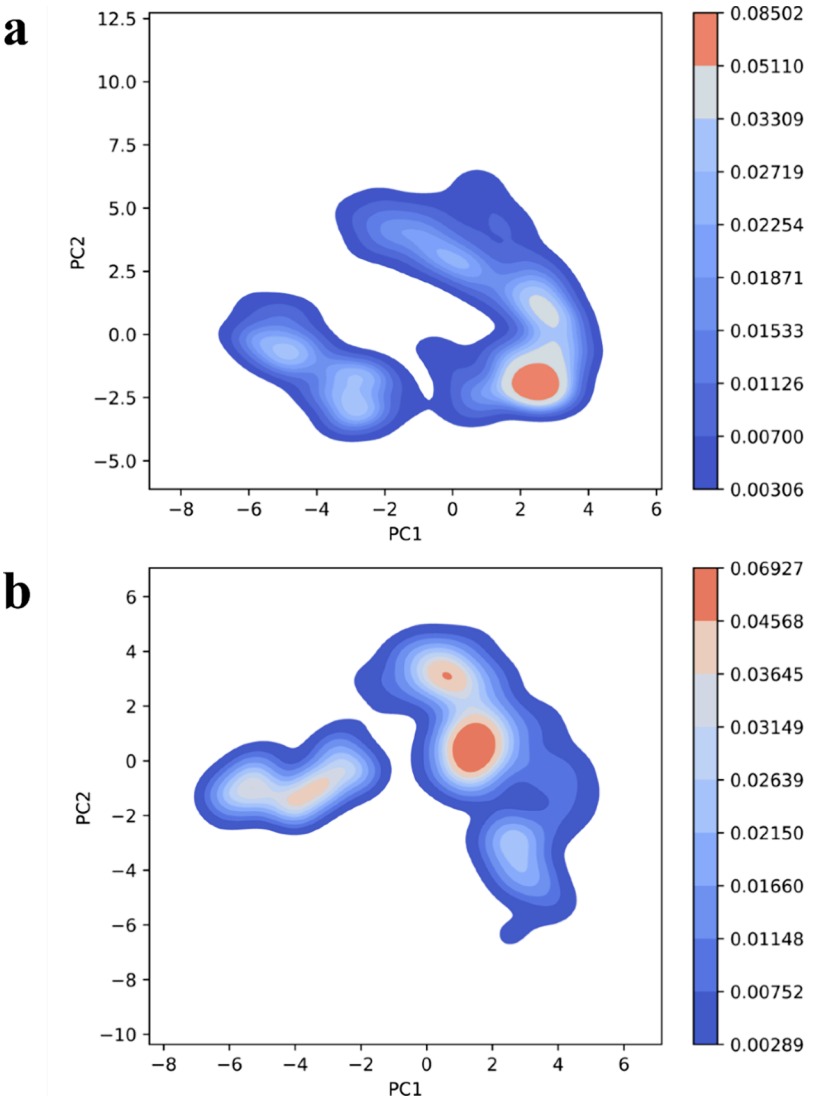

Figure 10. Gibbs free energy landscape plot of (a) HBD-2/4XCT (b) HBD-2/2I0E.

and is represented in Supp-Figure S1a and S1b, with eigenvector indices. In the case of both complexes, the first few eigenvalues relative to the concerted motions define the essential subspace, where the majority of the motions take place. In addition, the eigenvalues were observed to decrease in amplitude to reach more localized fluctuations and constrained numbers, indicative of structural constraints and stabilization within the complexes (Figure 9a and 9b).

Furthermore, the deviations found during PC analysis were assessed by computing free energy landscape (FEL) studies. FEL analysis is crucial for understanding the conformational changes and stability of biomolecules in relation to free energy changes during protein−protein interactions and complex formation. The blue regions (higher ΔGbind) favor an unfolding state of the protein, whereas the red spots indicate a more compact and folding state of the protein. The FEL plots clearly revealed that the two complexes presented relatively high ΔGbind values or blue spots (Figures 10a and 10b), which indicate structural flexibility and stabilization during the interaction.

Furthermore, these complexes equilibrated with high coverage of eigenvectors. Almost >95% of the total fluctuations were due to residues in the protein−protein interface. These results can be correlated with physiological conditions, as both complexes might have formed more frequently and attained greater degrees of stability. To visualize a simple, conformational landscape, different frames with similar conformations were grouped and analyzed. The RMSD values relative to the native bound structure were also calculated over the 1000 ns trajectory, providing insights into the stability and structural consistency of each complex throughout the simulation (Supp-Figure 2a and 2b).

4. CONCLUSIONS

In summary, this study provides an in-depth characterization of the structural properties, interaction stability, and dynamic features of HBD-2 in complex with MMP-9 and PKC-βII through advanced computational methods. These results suggest that the amino acid residues present at the protein−protein interface that participate in the interactions are vital for the functional activity of the receptors. The docking results were astonishing, as HBD-2 demonstrated a significant Z score with both the receptors MMP-9 and PKC-βII. The binding affinity was further substantiated by MD simulation studies. The RMSD, RMSF, SASA, ΔGbind, PC analysis and FEL analysis clearly demonstrated the structural and behavioral

https://doi.org/10.1021/acsomega.4c08292
ACS Omega 2025, 10, 3575−3584

changes of the residues during the MD study, which can directly correlate with the physiological behavior of proteins. These findings underscore the potential of HBD-2 as a dual inhibitor of MMP-9 and PKC-βII, suggesting that HBD-2 could effectively regulate pathways that are often dysregulated in chronic, nonhealing wounds associated with diabetes. By modulating these targets, HBD-2 has the potential to promote a balanced inflammatory response and support tissue regeneration, crucial steps for effective wound closure. Thus, HBD-2 has emerged as a promising candidate for therapeutic development, with its targeted action offering a novel strategy to accelerate DW healing. This study provides initial computational insights that lay the groundwork for future research, beginning with necessary in vitro and in vivo validation of the interaction between HBD-2 and MMP-9/PKC-βII.

■ ASSOCIATED CONTENT

Data Availability Statement

Available in the Supporting Information.

Supporting Information

The Supporting Information is available free of charge at https://pubs.acs.org/doi/10.1021/acsomega.4c08292.

The Supporting Information offers additional insights into the protein protein interaction analysis. Specifically figures S1 (a) and (b) depict eigenvalues and eigenvector index obtained through principal component analysis, highlighting the dominant modes of action. Figures S2 (a) and (b) show free energy landscape of the protein protein interactions, demonstrating the energetically favorable confirmations and binding pathways. These supporting figures complement the main text and provide a deeper understanding of the protein protein interaction dynamics (PDF)

■ AUTHOR INFORMATION

Corresponding Authors

Richie R. Bhandare − *Department of Pharmaceutical Sciences, College of Pharmacy & Health Sciences and Center of Medical and Bioallied Health Sciences Research, Ajman University, Ajman 340, UAE*; Email: r.bhandareh@ajman.ac.ae

Bharat Kumar Reddy Sanapalli − *Department of Pharmacology, School of Pharmacy & Technology Management, SVKM's Narsee Monjee Institute of Management Studies (NMIMS) Deemed to be University, Jadcherla, Telangana 509301, India*; orcid.org/0000-0002-9162-5553; Email: bharathsanapalli@yahoo.in

Authors

Vidyasrilekha Sanapalli − *Department of Pharmaceutical Chemistry, School of Pharmacy & Technology Management, SVKM's Narsee Monjee Institute of Management Studies (NMIMS) Deemed to be University, Jadcherla, Telangana 509301, India*; orcid.org/0000-0001-8298-1161

Dilep Kumar Sigalapalli − *Department of Pharmaceutical Chemistry, Vignan Pharmacy College, Jawaharlal Nehru Technological University, Guntur, Andhra Pradesh 522213, India*; Present Address: Current Address: Department of Biochemistry, University of Washington, Seattle, WA, US 98195

Afzal B. Shaik − *Department of Pharmaceutical Sciences, School of Biotechnology and Pharmaceutical Sciences, Vignan's Foundation for Science, Technology & Research, Guntur, Andhra Pradesh 522212, India; Center for Global Health Research, Saveetha Medical College, Saveetha Institute of Medical and Technical Sciences, Chennai, Tamil Nadu 600077, India*; orcid.org/0000-0002-9036-1963

Complete contact information is available at: https://pubs.acs.org/10.1021/acsomega.4c08292

Author Contributions

Vidyasrilekha. Sanapalli: Writing-Original Draft, Data Curation, Software, Validation; **Dilep Kumar. Sigalapalli:** Writing-Reviewing and editing, Formal Analysis; **Afzal B. Shaik:** Reviewing and editing; **Richie R. Bhandare:** Reviewing and editing; Funding Acquisition; **Bharat Kumar Reddy. Sanapalli:** Writing-Reviewing and editing, Conceptualization and Supervision.

Funding

This research did not receive any specific grant from funding agencies in the public, commercial, or not-for-profit sectors.

Notes

The authors declare no competing financial interest.

■ ACKNOWLEDGMENTS

RRB would like to thank Deanship of Graduate Studies and Research, Ajman University for providing article processing fees for this manuscript.

■ REFERENCES

(1) Prentki, M.; Nolan, C. J. Islet β cell failure in type 2 diabetes. *J. Clin. Invest.* **2006**, *116*, 1802−1812.

(2) Anselmo, M. I.; Nery, M.; Parisi, M. C. The effectiveness of educational practice in diabetic foot: a view from Brazil. *Diabetol. Metab. Synd.* **2010**, *2*, 1−4.

(3) Jirkovska, A. Basic questions in therapy of the diabetic foot. *Vnitrni Lekarstvi* **2002**, *48*, 542−548.

(4) Naves, C. C. The diabetic foot: a historical overview and gaps in current treatment. *Advances in wound care* **2016**, *5*, 191−197.

(5) Kolimi, P.; Narala, S.; Nyavanandi, D.; Youssef, A. A. A.; Dudhipala, N. Innovative treatment strategies to accelerate wound healing: trajectory and recent advancements. *Cells* **2022**, *11*, 2439.

(6) Mishra, A.; Kushare, A.; Gupta, M. N.; Ambre, P. Advanced Dressings for Chronic Wound Management. *ACS Appl. Bio Mater.* **2024**, 2660.

(7) Oliveira, A.; Simões, S.; Ascenso, A.; Reis, C. P. Therapeutic advances in wound healing. *Journal of Dermatological Treatment* **2022**, *33*, 2−22.

(8) Sethuram, L.; Thomas, J.; Mukherjee, A.; Chandrasekaran, N. A review on contemporary nanomaterial-based therapeutics for the treatment of diabetic foot ulcers (DFUs) with special reference to the Indian scenario. *Nanoscale Advances* **2022**, *4*, 2367−2398.

(9) Lipsky, B. A.; Berendt, A. R.; Cornia, P. B.; Pile, J. C.; Peters, E. J. G.; Armstrong, D. G.; Deery, H. G.; Embil, J. M.; Joseph, W. S.; Karchmer, A. W.; Pinzur, M. S.; Senneville, E. 2012 Infectious Diseases Society of America clinical practice guideline for the diagnosis and treatment of diabetic foot infections. *Clin. Infect. Dis.* **2012**, *54*, e132−e173.

(10) Demidova-Rice, T. N.; Durham, J. T.; Herman, I. M. Wound healing angiogenesis: innovations and challenges in acute and chronic wound healing. *Advances in wound care* **2012**, *1*, 17−22.

(11) Ryckman, C.; Gilbert, C.; de Médicis, R.; Lussier, A.; Vandal, K.; Tessier, P. A. Monosodium urate monohydrate crystals induce the release of the proinflammatory protein S100A8/A9 from neutrophils. *Journal of leukocyte biology* **2004**, *76*, 433−440.

(12) Busso, N.; So, A. Gout. Mechanisms of inflammation in gout. *Arthritis Res. Ther.* **2010**, *12*, 206.
(13) Wong, S. L.; Demers, M.; Martinod, K.; Gallant, M.; Wang, Y.; Goldfine, A. B.; Kahn, C. R.; Wagner, D. D. Diabetes primes neutrophils to undergo NETosis, which impairs wound healing. *Nature medicine* **2015**, *21*, 815−819.
(14) Fadini, G. P.; Menegazzo, L.; Rigato, M.; Scattolini, V.; Poncina, N.; Bruttocao, A.; Ciciliot, S.; Mammano, F.; Ciubotaru, C. D.; Brocco, E.; Marescotti, M. C.; Cappellari, R.; Arrigoni, G.; Millioni, R.; Vigili de Kreutzenberg, S.; Albiero, M.; Avogaro, A. NETosis delays diabetic wound healing in mice and humans. *Diabetes* **2016**, *65*, 1061−1071.
(15) Wang, F.; Huang, D.; Zhu, W.; Li, S.; Yan, M.; Wei, M.; Li, J. Selective inhibition of PKCβ2 preserves cardiac function after myocardial infarction and is associated with improved angiogenesis of ischemic myocardium in diabetic rats. *International journal of molecular medicine* **2013**, *32*, 1037−1046.
(16) Huang, D.; Wang, F.-B.; Guo, M.; Li, S.; Yan, M.-L.; Yu, T.; Wei, M.; Li, J.-B. Effect of combined treatment with rosuvastatin and protein kinase Cβ2 inhibitor on angiogenesis following myocardial infarction in diabetic rats. *Int. J. Mol. Med.* **2015**, *35*, 829−838.
(17) Gray, R. D.; Lucas, C. D.; MacKellar, A.; Li, F.; Hiersemenzel, K.; Haslett, C.; Davidson, D. J.; Rossi, A. G. Activation of conventional protein kinase C (PKC) is critical in the generation of human neutrophil extracellular traps. *Journal of inflammation* **2013**, *10*, 12−8.
(18) Fadini, G.; Menegazzo, L.; Scattolini, V.; Gintoli, M.; Albiero, M.; Avogaro, A. A perspective on NETosis in diabetes and cardiometabolic disorders. *Nutrition, Metabolism and Cardiovascular Diseases* **2016**, *26*, 1−8.
(19) DEKKER, L. V.; LEITGES, M.; ALTSCHULER, G.; MISTRY, N.; MCDERMOTT, A.; ROES, J.; SEGAL, A. W. Protein kinase C-β contributes to NADPH oxidase activation in neutrophils. *Biochem. J.* **2000**, *347*, 285−289.
(20) Neeli, I.; Radic, M. Opposition between PKC isoforms regulates histone deimination and neutrophil extracellular chromatin release. *Front. Immunol.* **2013**, *4*, 38.
(21) Jones, J. I.; Nguyen, T. T.; Peng, Z.; Chang, M. Targeting MMP-9 in diabetic foot ulcers. *Pharmaceuticals* **2019**, *12*, 79.
(22) McLennan, S.; Yue, D.; Twigg, S., Molecular aspects of wound healing in diabetes. *Primary Intention*; The Australian Journal of Wound Management **2006**, *14*.
(23) Ambrozova, N.; Ulrichova, J.; Galandakova, A., *Models for the study of skin wound healing. The role of Nrf2 and NF-κB*. Biomedical Papers of the Medical Faculty of Palacky University in Olomouc **2017**, *161*.
(24) Fjell, C. D.; Hiss, J. A.; Hancock, R. E.; Schneider, G. Designing antimicrobial peptides: form follows function. *Nat. Rev. Drug Discovery* **2012**, *11*, 37−51.
(25) Mohanty, T.; Alberius, P.; Schmidtchen, A.; Reiss, K.; Schröder, J.; Sørensen, O. E. Saliva induces expression of antimicrobial peptides and promotes intracellular killing of bacteria in keratinocytes by epidermal growth factor receptor transactivation. *Brit. J. Dermatol.* **2017**, *176*, 403−412.
(26) Baroni, A.; Donnarumma, G.; Paoletti, I.; Longanesi-Cattani, I.; Bifulco, K.; Tufano, M. A.; Carriero, M. V. Antimicrobial human beta-defensin-2 stimulates migration, proliferation and tube formation of human umbilical vein endothelial cells. *Peptides* **2009**, *30*, 267−272.
(27) Griffith, G. L.; Kasus-Jacobi, A.; Pereira, H. A. Bioactive antimicrobial peptides as therapeutics for corneal wounds and infections. *Advances in wound care* **2017**, *6*, 175−190.
(28) Niyonsaba, F.; Nagaoka, I.; Ogawa, H.; Okumura, K. Multifunctional antimicrobial proteins and peptides: natural activators of immune systems. *Current pharmaceutical design* **2009**, *15*, 2393−2413.
(29) Schneider, J. J.; Unholzer, A.; Schaller, M.; Schäfer-Korting, M.; Korting, H. C. Human defensins. *Journal of molecular medicine* **2005**, *83*, 587−595.
(30) Spencer, J. D.; Hains, D. S.; Porter, E.; Bevins, C. L.; DiRosario, J.; Becknell, B.; Wang, H.; Schwaderer, A. L. Human alpha defensin 5 expression in the human kidney and urinary tract. *PloS one* **2012**, *7*, No. e31712.
(31) Bruhn, O.; Grötzinger, J.; Cascorbi, I.; Jung, S. Antimicrobial peptides and proteins of the horse-insights into a well-armed organism. *Vet. Res.* **2011**, *42*, 98.
(32) Corrales-Garcia, L.; Ortiz, E.; Castañeda-Delgado, J.; Rivas-Santiago, B.; Corzo, G. Bacterial expression and antibiotic activities of recombinant variants of human β-defensins on pathogenic bacteria and M. tuberculosis. *Protein Expression Purif.* **2013**, *89*, 33−43.
(33) Machado, L. R.; Ottolini, B. An evolutionary history of defensins: a role for copy number variation in maximizing host innate and adaptive immune responses. *Front. Immunol.* **2015**, *6*, 115.
(34) Hans, M.; Madaan Hans, V. Epithelial antimicrobial peptides: guardian of the oral cavity. *Int. J. Peptides* **2014**, *2014*, 370297.
(35) Underwood, M.; Bakaletz, L. Innate immunity and the role of defensins in otitis media. *Curr. Allergy Asthma Rep.* **2011**, *11*, 499−507.
(36) Laskowski, R. A.; MacArthur, M. W.; Moss, D. S.; Thornton, J. M. PROCHECK: a program to check the stereochemical quality of protein structures. *Journal of applied crystallography* **1993**, *26*, 283−291.
(37) Wiederstein, M.; Sippl, M. J. ProSA-web: interactive web service for the recognition of errors in three-dimensional structures of proteins. *Nucleic acids research* **2007**, *35*, W407−W410.
(38) Schüttelkopf, A. W.; Van Aalten, D. M. PRODRG: a tool for high-throughput crystallography of protein−ligand complexes. *Acta Crystallographica Section D: Biological Crystallography* **2004**, *60*, 1355−1363.
(39) Gangadharappa, B. S.; Sharath, R.; Revanasiddappa, P. D.; Chandramohan, V.; Balasubramaniam, M.; Vardhineni, T. P. Structural insights of metallo-beta-lactamase revealed an effective way of inhibition of enzyme by natural inhibitors. *J. Biomol. Struct. Dyn.* **2020**, *38*, 3757−3771.
(40) Prasanth, D.; Murahari, M.; Chandramohan, V.; Panda, S. P.; Atmakuri, L. R.; Guntupalli, C. In silico identification of potential inhibitors from Cinnamon against main protease and spike glycoprotein of SARS CoV-2. *J. Biomol. Struct. Dyn.* **2021**, *39*, 4618−4632.
(41) Kumari, R.; Kumar, R.; Lynn, A. g_mmpbsa— A GROMACS tool for high-throughput MM-PBSA calculations. *J. Chem. Inf. Model.* **2014**, *54*, 1951−1962.
(42) Ringnér, M. What is principal component analysis? *Nature biotechnology* **2008**, *26*, 303−304.
(43) Amadei, A.; Linssen, A. B.; Berendsen, H. J. Essential dynamics of proteins. *Proteins: Struct., Funct., Bioinf.* **1993**, *17*, 412−425.
(44) Maisuradze, G. G.; Leitner, D. M. Free energy landscape of a biomolecule in dihedral principal component space: Sampling convergence and correspondence between structures and minima. *Proteins: Struct., Funct., Bioinf.* **2007**, *67*, 569−578.
(45) Hess, B. Similarities between principal components of protein dynamics and random diffusion. *Phys. Rev. E* **2000**, *62*, 8438.
(46) Amadei, A.; Ceruso, M. A.; Di Nola, A. On the convergence of the conformational coordinates basis set obtained by the essential dynamics analysis of proteins' molecular dynamics simulations. *Proteins: Struct., Funct., Bioinf.* **1999**, *36*, 419−424.
(47) Pontiggia, F.; Colombo, G.; Micheletti, C.; Orland, H. Anharmonicity and self-similarity of the free energy landscape of protein G. *Physical review letters* **2007**, *98*, No. 048102.

https://doi.org/10.1021/acsomega.4c08292
ACS Omega 2025, 10, 3575−3584